Broken symmetry states of metallacrowns: Distribution of spins and the *g* tensor

Y. Pavlyukh,[1,2,*] E. Rentschler,[3] H. J. Elmers,[4] W. Hübner,[1] and G. Lefkidis[1]
[1]*Department of Physics and Research Center OPTIMAS, Technische Universität Kaiserslautern, P.O. Box 3049, 67653 Kaiserslautern, Germany*
[2]*Institut für Physik, Martin-Luther-Universität Halle-Wittenberg, 06120 Halle, Germany*
[3]*Institut für Anorganische und Analytische Chemie, Universität Mainz, D-55128 Mainz, Germany*
[4]*Institut für Physik, Johannes Gutenberg-Universität Mainz, D-55128 Mainz, Germany*

(Received 22 August 2018; revised manuscript received 1 April 2019; published 19 April 2019)

In this work we focus on the magnetic properties of metallacrown complexes as computed by various density functional methods. Using the broken symmetry approach, we determine the exchange-coupling constants and the *g* tensors and compare them with experimentally determined ones from the temperature-dependent magnetic susceptibilities and by the electronic spin resonance, respectively. Generalization of the Noodleman-Dai-Whangbo approach for systems with multiple magnetic centers that we introduce here allows to make quantitative statements about the nature of these electronic states in density functional theory.

DOI: 10.1103/PhysRevB.99.144418

I. INTRODUCTION

Partially filled electronic states give raise to magnetic moments, exchange interactions, and magnetism. In addition, relativistic effects modify the picture, give rise to the *g* tensor, and are related to the onset of magnetocrystalline anisotropy in molecular systems. Depending on the character of the exchange interaction, the magnetic coupling can be either ferromagnetic (FM) or antiferromagnetic (AFM). In the first case, a parallel spin orientation is favored, leading to a high-spin electron configuration [1]. However, in many systems, especially in molecular magnets [2,3], the AFM coupling dominates [4]. It originates from a variety of superexchange mechanisms that favor open-shell low-spin electron configurations [5–7]. It is not possible to describe such electronic states within the conventional density functional theory (DFT) because, for a given number of spin-up and -down electrons, the theory only targets states of the highest possible multiplicity.

Different *ab initio* approaches can be used [8]. In our previous work [9], we applied the complete active space (CAS) quantum chemistry method to study magnetism in two prominent metallacrown (MC) molecules [10]. We demonstrated that the full set of electronic states responsible for magnetism can be computed and mapped onto the isotropic exchange Heisenberg-Dirac-Van Vleck Hamiltonian leading to the determination of the exchange-coupling constants (J_{ij}). While correctly predicting the sign of magnetic interactions and the multiplicity of the ground state, we found that computed numerical values deviated from the experimental ones. We furthermore showed that the agreement with experiment can be improved by taking the dynamical electron correlations into account. This can be done, for instance, by using the so-called *N*-electron valence state perturbation theory on top of the CAS electronic state. Similar conclusions were obtained for the cluster representation of periodic systems [11]. For smaller systems, it is possible to use multireference methods such as the multireference coupled-cluster (MR-CC) approach [12]. However, with increasing system size, it soon becomes impractical.

Therefore, in this work, we address the same systems using a combination of the density functional theory and the so-called *broken symmetry approach* to study their magnetic properties. This approach has a long (preceding the discovery of density functional theory) and fruitful history as it allows to describe with minimal cost a range of phenomena using the Slater determinant as an ansatz for the many-body wave function. One can classify the Slater determinants as *restricted* preserving S^2 and S_z spin symmetry, *unrestricted* that break the S^2 symmetry, generalized (S^2 and S_z are not good quantum numbers), and such that do not preserve the particle number as in the Bardeen-Cooper-Schrieffer theory. Focusing on the unrestricted level and molecular spin systems, there are three approaches to deal with the broken symmetry (BS) states that lead to meaningful properties. First, we briefly summarize them regarding the Hartree-Fock and Kohn-Sham theories on equal footing. We are well aware of some conceptual differences between these two theories. Here, we emphasize their single-determinant nature.

The first possibility is the *projection* technique proposed by Löwdin [13] and refined by many authors [14]. A fundamental insight into the nature of an unrestricted Hartree-Fock (UHF) state is provided by the Thouless theorem [15], stating that it can be obtained by a unitary transformation of the associated restricted Hartree-Fock state. This state can be further purified to yield the desired spin symmetry by applying a spin-projection operator (singlet projection operators are commonly used).

The second possibility is to use the broken symmetry state without a projection, but properly account for the expectation values of the spin-squared operator $\langle \hat{\mathbf{S}}^2 \rangle$ for the determination of J_{ij}. This approach was originated by Noodleman and

*pavlyukh@physik.uni-kl.de

Davidson [16]. They considered a system with two magnetic centers and have shown that J can be computed provided the overlap between the half-filled orbitals is known. For vanishing overlap (as in the restricted open-shell solution or if spatial degrees of freedom are not taken into account), the theory was extended toward a general number of electrons forming the spin state and was put on solid theoretical ground by Dai and Whangbo [17]. Dai and Whangbo give a formula for $\langle \hat{\mathbf{S}}^2 \rangle$ in terms of the number of unpaired electrons on the two sites (m and n, respectively). In particular, they obtain that

$$\langle \hat{\mathbf{S}}^2 \rangle = \tfrac{1}{4}(m-n)^2 + \tfrac{1}{2}(m+n). \quad (1)$$

Knowing the expansion of BS states in terms of the $\hat{\mathbf{S}}^2$ eigenstates, formulas for energies can be given as well, which allows for the determination of J. Somewhat in contrast to this methodology is the approach of Ruiz *et al.* [18] (here, in contrast to the earlier works, the applicability of the BS approach was considered and a convenient expression for the overlap in terms of the onsite spin densities was derived), where a suggestion to use the states from BS DFT *without a projection* was put forward. The work of Perdew *et al.* [19] is used as a justification: the spin density from DFT is not a well-defined property and the Kohn-Sham determinant need not be an eigenfunction of the total spin squared $\hat{\mathbf{S}}^2$ [20]. Instead, it has been suggested that the on-top electron pair density is the relevant physical observable. Numerous applications of the Ruiz method (He-bridged H benchmark systems, polynuclear transition metal complexes [21], or the Fe_{19} complex [22]) have in common a postulate that for the determination of n distinct exchange constants J_{ij} only $n+1$ energies (typically a high-spin and n BS solutions) are required. This approach is not unique: Kortus *et al.* [23] have used a redundant set of determining equations (13 states) and the least-squares fitting to find 6 exchange interaction constants in the V_{15} spin system. Bellini and Affronte used a slight variation that involved averaging in order to study Cr_8 and Cr_7M rings [24] and their dimers [25]. Chiesa *et al.* [26,27] studied similar ring systems, by mapping onto an extended Hubbard model in the basis of Foster-Boys orbitals, the so-called DFT + many-body approach.

Because the fitting was on the Ising model level, the need of assigning a meaningful physical state to each broken symmetry solution was eliminated, however, without solving the conceptual problem. A further attempt that stirred hot debates was a suggestion of Ruiz *et al.* [28] that spin projection must only be used in conjunction with the self-interaction correction of the approximate density functional. In contrast and according to Adamo *et al.* [29], the self-interaction error is inherent to all exchange-correlation potentials irrespective of the approach used to include the spin symmetry.

The third possibility, which lies within the realm of DFT, is to extend the variational search to include states with fractional occupations [30]. Practical implementations are known as spin-restricted open-shell KS (ROKS) [31] and spin-restricted ensemble-referenced KS (REKS) [32] methods. They can be regarded as generalizations of the CASSCF approach to the Kohn-Sham scheme (by no means unique [33], see also recent developments on pair density functional theory [34,35]), however, due to a difference in the treatment of dynamical correlations, the two approaches are not equivalent even if the exchange-correlation functional is restricted to the exchange-only case [36]. However, despite a solid foundation, Illas *et al.* [37] compared unrestricted and spin-restricted ensemble referenced methods and found that the results do not follow a systematic trend [in contrast to complete-active-space self-consistent-field (CASSCF) which is known to underestimate J, but behaves predictably]. This was attributed to the insufficiency of the contemporary density functionals: "DFT can provide seemingly accurate numerical results but for the wrong physical reasons" [37].

Under these circumstances, is everything so hopeless with DFT in description of magnetic properties as described in the work of Illas *et al.* [37]? Noodleman's prescription has been tested for many systems at the DFT level. While it does contain some arbitrariness related to the unknown overlap, the results are encouraging [17]. In other studies, the Noodleman-Dai-Whangbo approach has been compared with experimental data, or with other theories. However, they do not address the concerns of Illas *et al.* that the discrepancies are due to erratic behavior of the density functionals.

In this work we describe an approach that can conclusively address these doubts, and upon the application to two MC molecules, we rigorously establish that DFT results for the exchange coupling constants are generally consistent. Aside from this basic magnetic property, we also focus on the experimentally relevant relativistic parameter such as the g tensor. This property has been scarcely discussed in relation to the broken symmetry states. Therefore, we develop a general formalism for the determination of g from the combination of BS solutions and numerically demonstrate that results are likewise consistent. Measurements for the two systems have been performed at Heidelberg University and reported by Park [38] and in Ref. [39].

Systems with more than two magnetic centers are generally perceived as very complex [40–42]. However, exactly due to this fact a multitude of BS states (exceeding the number of anticipated exchange constants such as shown in Fig. 1) can be obtained. This redundancy, which is not available for two magnetic centers, allows us to test the internal consistency of the broken symmetry Kohn-Sham theories without resorting to the Ising model as was done by Kortus *et al.* [23].

We organize our work in the following way: In Sec. II A general information about the coupling of spin or angular moments is presented. Note that this operation is *nonassociative* and therefore depends on the order in which the momenta are added. This mathematical intricacy never comes into play in systems with two magnetic centers, as mentioned above. However, it is essential for the present discussion. This general theory needs to be specialized for the two exemplary systems that we study (Secs. II B and II C). We apply our method to two representative MC molecules: $Cu^{II}(DMF)_2\ Cl_2[12\text{–}MC_{Fe^{III}N(Shi)}\ 4](DMF)_4$ and $(HNEt_3)_2Cu^{II}[12\text{–}MC_{Cu^{II}N(Shi)}\ 4]$ metallacrowns ({$CuFe_4$} and {$CuCu_4$} for brevity; in the full metallacrown notation, as introduced by Pecoraro, 12 refers to the total number of segments in the cyclic host, and 4 is the number of involved oxygen atoms [4,43]). Therefore, we discuss the exchange coupling of 5 spins (AB_4) and generalize results of Dai and Whangbo for exactly this scenario (see Fig. 1 for the visualization of spin density of the {$CuFe_4$}

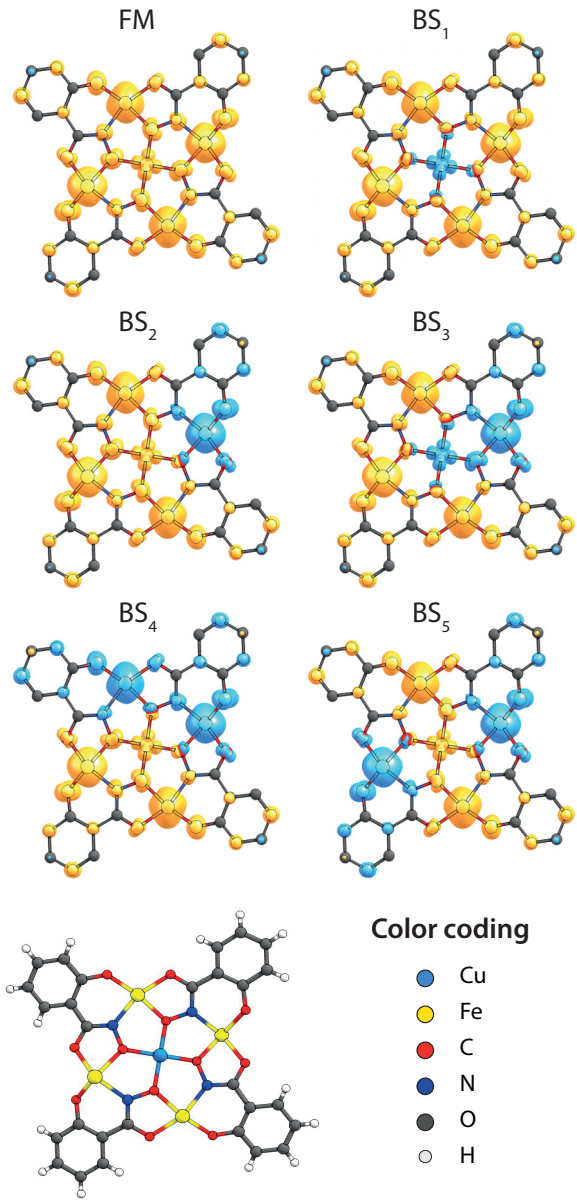

FIG. 1. Spin density of the $CuFe_4$ heterometallic molecule for the states presented in Table II (positive values: yellow, negative values: blue). Spin localization on the oxygen (A-O-B) and the oxamate (A-O-N-B) bridges connecting the central and the peripheral TM ions is a marked feature of the superexchange coupling mechanism [6]. In the first case, the spin-polarized density can be readily seen on the O atom, whereas in the second case, O and N atoms have different polarizations. Spin density localized on TM ions can be understood considering their electronic configurations: d^9 for Cu^{II} and d^5 for Fe^{III}. The hole on Cu^{II} is primarily located on the $d_{x^2-y^2}$ orbital; therefore, the four lobes are pointing toward Fe^{III} ions as observed in our previous study [9]. At variance, spin density on the peripheral Fe^{III} ions is formed by all five d orbitals. It has a distorted spherical shape reflecting the local approximate octahedral symmetry.

system). For the given molecules, the relativistic energy-level splitting is smaller than that due to spin-exchange interactions. This allows us to consider the Zeeman splitting on top. In Sec. II D we develop a theory of the g tensor for broken symmetry states. This rests on the ideas known from the treatment of pure spin systems by Bencini and Gatteschi [44,45], and on the investigation of a spin dimer by Slep *et al.* [46]. Finally, in Sec. II E we go into the details of our *ab initio* approach. We present comparative results for a variety of exchange-correlation functionals that are representatives of different families: generalized gradient approximation (GGA), hybrid (with admixture of Hartree-Fock exchange), and meta-GGA in Sec. III. A general overview of these functionals and of the relativistic options for the state optimizations and for the calculation of spin-orbit coupling, which is a particularly important ingredient of the g-tensor calculations, can be found in the Supplemental Material [47].

II. THEORY

This section deals with three aspects of our method: the formal approach to spin or angular momentum coupling, the determination of the g tensor for systems in the strong exchange-coupling limit on the basis of BS calculations, and the *ab initio* approach.

A. Coupling of spins

In the work of Dai and Whangbo [48], a two-center system (AB) with m unpaired electrons at site A and n unpaired electrons at site B was considered. It contains in total $(n+1)$ $(m+1)$ spin states. Assuming without losing generality that $m > n$, we can obtain these states by the application of n spin-flip operators acting on the electronic states on site B. Already at this point it is evident that these electronic states must be localized on the respective sites, a property that can not be guaranteed in general. The antisymmetrized products of these single-particle states form the many-body Slater determinants. They are not the eigenfunctions of the Heisenberg spin Hamiltonian and they do not possess a well-defined total spin. The authors derive this conclusion from the expansion of the direct product of two spin states with total spins s_A and s_B and their z components m_A and m_B, respectively:

$$|s_A m_A\rangle|s_B m_B\rangle = \sum_{s=|s_A-s_B|}^{s_A+s_B} (-1)^{-s_A+s_B-m}\sqrt{2s+1} \times \begin{pmatrix} s_A & s_B & s \\ m_A & m_B & -m \end{pmatrix} |sm\rangle. \quad (2)$$

Here, the round brackets stand for the Wigner $3j$ symbols. Due to their orthogonality, Eq. (2) can also be inverted, yielding the expansion of the composite state of the AB system in terms of its constituents.

While this equation perfectly suits its purpose of deriving the energy and other observables for the broken symmetry state, it misses one important ingredient that does not even come into play for two magnetic centers. In writing $|sm\rangle$, information about the spin moments of participating states, i.e., s_A and s_B is not manifestly indicated. A completely equivalent expression to Eq. (2) would be

$$|s_A m_A\rangle|s_B m_B\rangle = \sum_{s=|s_A-s_B|}^{s_A+s_B} C^{sm}_{s_A m_A\, s_B m_B} |s_A s_B sm\rangle, \quad (3)$$

where the projection of angular momentum fulfills $m = m_A + m_B$. Here, we used the Clebsch-Gordan coefficient and took the missing indices into account. Upon exchange of two particles, the Clebsch-Gordan coefficient changes the sign:

$$C^{lm}_{l_1 m_1\, l_2 m_2} = (-1)^{l_1+l_2-l} C^{lm}_{l_2 m_2\, l_1 m_1}. \tag{4}$$

We will return to this important fact later.

In order to understand why is it important to keep the information about intermediate states, let us turn to a more general situation where three angular momenta are sequentially added: the result of such addition depends on the order in which states are coupled and what are the intermediate states of the composite system. The transformation between different representations is performed by the $6j$ symbols:

$$\langle l_1 l_2 (l_{12}) l_3 l m | l_1 l_3 (l_{13}) l_2 l' m' \rangle = \delta_{ll'}\delta_{mm'}(-1)^{l_1+l_2+l_3+l}\sqrt{(2l_{12}+1)(2l_{13}+1)}\begin{Bmatrix} l_1 & l_2 & l_{12} \\ l_3 & l & l_{13} \end{Bmatrix}. \tag{5}$$

Mathematically, this means that for the case of representations of a finite group, the character table, together with its $6j$ symbols, uniquely determines the group up to isomorphism, while the character table alone does not. In the case of four particles, $9j$ symbols can be used and so on.

Let us formulate general notations for the addition of n spins $\{s_1, s_2, \ldots, s_n\}$. The order in which Eq. (2) is applied matters and can be indicated as follows:

$$|s_a m_a, \{s_A\}\rangle |s_b m_b, \{s_B\}\rangle = \sum_{s_0=|s_a-s_b|}^{s_a+s_b} (-1)^{-s_a+s_b-m_0}\sqrt{2s_0+1}\begin{pmatrix} s_a & s_b & s_0 \\ m_a & m_b & -m_0 \end{pmatrix} |s_0 m_0, \{s_a, s_A, s_b, s_B\}\rangle. \tag{6}$$

It is convenient to choose the set of spins $\{s_A\}$ to be empty (i. e., we are adding momenta one by one), therefore, the final state can be indicated without the use of parathesis $|s_0 m_0, \{s_1, s_2, \ldots, s_n\}\rangle$, where we renumber $\{s_1, s_2, \ldots, s_n\} = \{s_a, s_A, s_b, s_B\}$. The state in Eq. (6) results from the following sequence of additions:

$$\mathbf{s}_{n-2} = \mathbf{s}_{n-1} + \mathbf{s}_n, \quad \mathbf{s}_{n-4} = \mathbf{s}_{n-3} + \mathbf{s}_{n-2}, \ldots \quad \mathbf{s}_0 = \mathbf{s}_1 + \mathbf{s}_2.$$

Addition of spins can be conveniently performed using a computer algebra system such as MATHEMATICA.

An important aspect in the application to AB_4 spin systems is the fact that the order of additions has to match the energy solutions. In the square-symmetric geometry, which is assumed throughout the text, with the isotropic exchange (ex) the Heisenberg-Dirac-Van Vleck Hamiltonian [3] is given by

$$\widehat{\mathcal{H}}_{\rm ex} = -2J_1 \sum_i \hat{\mathbf{s}}_A \cdot \hat{\mathbf{s}}_{B_i} - 2J_2 \sum_{\langle ij \rangle} \hat{\mathbf{s}}_{B_i} \cdot \hat{\mathbf{s}}_{B_j}, \tag{7}$$

where $\langle ij \rangle$ denotes a collection of nearest neighbors. $\hat{\mathbf{s}}_A$ and $\hat{\mathbf{s}}_{B_i}$ are effective spin operators representing possibly composite spins on the centers A and B_i, respectively. The eigenenergies can be expressed in terms of the total spin $\hat{\mathbf{S}} = \hat{\mathbf{s}}_A + \hat{\mathbf{S}}_B$, and three additional quantum numbers: $\hat{\mathbf{S}}_{13} = \hat{\mathbf{s}}_{B_1} + \hat{\mathbf{s}}_{B_3}$, $\hat{\mathbf{S}}_{24} = \hat{\mathbf{s}}_{B_2} + \hat{\mathbf{s}}_{B_4}$, and the total spin of the ring atoms $\hat{\mathbf{S}}_B = \hat{\mathbf{S}}_{13} + \hat{\mathbf{S}}_{24}$. The eigenstates are $|S_{13}, S_{24}, S_B, S, M_S\rangle$ and the corresponding energy is

$$\begin{aligned} &E(|S_{13}S_{24}S_B S M_S\rangle) \\ &\quad = -J_2[S_B(S_B+1) - S_{13}(S_{13}+1) - S_{24}(S_{24}+1)] \\ &\qquad - J_1[S(S+1) - s_A(s_A+1) - S_B(S_B+1)], \end{aligned} \tag{8}$$

where $S_k(S_k+1)$ is the expectation value of $\hat{\mathbf{S}}_k^2$, and M_S is the total spin projection. The system is degenerate with respect to this quantum number, therefore, it will be skipped in the designation of states. The dimension of the Hilbert space is $(2s_A+1)(2s_B+1)^4$.

From the solution (8), it is sensible that addition of spins with the goal of determining the BS states decomposition is performed in the following order:

$$\begin{aligned} &\hat{\mathbf{S}}_{13} = \hat{\mathbf{s}}_{B_1} + \hat{\mathbf{s}}_{B_3}, \quad \hat{\mathbf{S}}_{24} = \hat{\mathbf{s}}_{B_2} + \hat{\mathbf{s}}_{B_4}, \quad \hat{\mathbf{S}}_B = \hat{\mathbf{S}}_{13} + \hat{\mathbf{S}}_{24}, \\ &\hat{\mathbf{S}} = \hat{\mathbf{s}}_A + \hat{\mathbf{S}}_B. \end{aligned} \tag{9}$$

The reason is purely technical: it ensures that intermediate states are the eigenstates of the Hamiltonian (7) restricted to subsystems, allowing to easily determine energies of the BS states. For less symmetric systems, or for more spins the analytic solution may not be available. How is the addition of spins performed in this case?

The algorithm is still straightforward: the additions are performed in an arbitrary order keeping track of the intermediate configurations as indicated above (6). On the last step, a projection onto states with well-defined $\langle \hat{\mathbf{S}}^2 \rangle$ is performed.

For a general spin Hamiltonian $\widehat{\mathcal{H}}_{\rm ex} = -\sum_{a,b} J_{ab} \hat{\mathbf{s}}_a \cdot \hat{\mathbf{s}}_b$, the energy expectation values are computed by considering the matrix elements

$$2\langle {\rm BS}|\hat{\mathbf{s}}_a \cdot \hat{\mathbf{s}}_b|{\rm BS}\rangle = \langle {\rm BS}|(\hat{\mathbf{s}}_a + \hat{\mathbf{s}}_b)^2|{\rm BS}\rangle - \langle \hat{\mathbf{s}}_a^2 \rangle - \langle \hat{\mathbf{s}}_b^2 \rangle, \tag{10}$$

where the broken symmetry state is obtained by the application of the spin-flip operators

$$\hat{s}^{\pm}|s, m\rangle = \sqrt{s(s+1) - m(m \pm 1)}|s, m \pm 1\rangle \tag{11}$$

on the high-spin state as follows:

$$|{\rm BS}\rangle = \prod_{k \in \{F\}} \hat{s}_k^- |{\rm HS}\rangle. \tag{12}$$

Here, $\{F\}$ is a set of centers where the spin flip is performed. For obvious reasons, it is of advantage to perform the addition of interacting spins first. In general, the calculation can soon become tedious because each term of the Hamiltonian needs to be treated separately, and such a treatment can involve the addition of a large number of spins.

TABLE I. Excited states of the $CuCu_4$ system from the broken symmetry approach. Numerical data from the PBE0 DFT BS calculations. In the fourth column, a constant −10466.0 Hr is subtracted, the values in the fourth column are with respect to the BS_4 state. The least-squares fit yields $J_1 = -42.697$ meV and $J_2 = -13.856$ meV with the root-mean-square error $\delta_{\mathrm{RMSE}} = 0.430$ meV.

State	$\langle\hat{\mathbf{S}}^2\rangle$	$\langle\widehat{\mathcal{H}}_{\mathrm{ex}}\rangle$	E(Hr)	E (meV)	E^{fit} (meV)	Spin configuration $\lvert S_{13}, S_{24}, S_B, S\rangle$
HS = $\begin{bmatrix}\uparrow & & \uparrow\\ & \uparrow & \\ \uparrow & & \uparrow\end{bmatrix}$	$\frac{35}{4}$	$-2(J_1+J_2)$	−0.811967669	113.643	113.358	$\lvert 1,1,2,\frac{5}{2}\rangle$
BS_1 = $\begin{bmatrix}\uparrow & & \uparrow\\ & \downarrow & \\ \uparrow & & \uparrow\end{bmatrix}$	$\frac{19}{4}$	$2(J_1-J_2)$	−0.818264945	−57.715	−57.430	$\frac{1}{\sqrt{5}}\lvert 1,1,2,\frac{5}{2}\rangle + \frac{2}{\sqrt{5}}\lvert 1,1,2,\frac{3}{2}\rangle$
BS_2 = $\begin{bmatrix}\downarrow & & \uparrow\\ & \uparrow & \\ \uparrow & & \uparrow\end{bmatrix}$	$\frac{19}{4}$	$-J_1$	−0.814580762	42.537	42.970	$\frac{1}{\sqrt{5}}\lvert 1,1,2,\frac{5}{2}\rangle - \frac{1}{\sqrt{2}}\lvert 0,1,1,\frac{3}{2}\rangle - \frac{1}{2}\lvert 1,1,1,\frac{3}{2}\rangle - \frac{1}{2\sqrt{5}}\lvert 1,1,2,\frac{3}{2}\rangle$
BS_3 = $\begin{bmatrix}\downarrow & & \uparrow\\ & \downarrow & \\ \uparrow & & \uparrow\end{bmatrix}$	$\frac{11}{4}$	$2J_1$	−0.817677088	−41.718	−42.424	$\frac{1}{\sqrt{10}}\lvert 1,1,2,\frac{5}{2}\rangle + \frac{1}{2}\sqrt{\frac{3}{5}}\lvert 1,1,2,\frac{3}{2}\rangle - \frac{1}{2\sqrt{3}}\lvert 1,1,1,\frac{3}{2}\rangle - \frac{1}{\sqrt{6}}\lvert 0,1,1,\frac{3}{2}\rangle - \frac{1}{\sqrt{6}}\lvert 1,1,1,\frac{1}{2}\rangle - \frac{1}{\sqrt{3}}\lvert 0,1,1,\frac{1}{2}\rangle$
BS_4 = $\begin{bmatrix}\downarrow & & \downarrow\\ & \uparrow & \\ \uparrow & & \uparrow\end{bmatrix}$	$\frac{11}{4}$	0	−0.816143969	0.000	0.273	$\frac{1}{\sqrt{10}}\lvert 1,1,2,\frac{5}{2}\rangle - \frac{1}{\sqrt{6}}\lvert 0,1,1,\frac{3}{2}\rangle - \frac{1}{\sqrt{6}}\lvert 1,0,1,\frac{3}{2}\rangle - \frac{1}{\sqrt{15}}\lvert 1,1,2,\frac{3}{2}\rangle + \frac{1}{2\sqrt{3}}\lvert 1,0,1,\frac{1}{2}\rangle - \frac{1}{2\sqrt{3}}\lvert 1,1,0,\frac{1}{2}\rangle + \frac{1}{2\sqrt{3}}\lvert 0,1,1,\frac{1}{2}\rangle + \frac{1}{2}\lvert 0,0,0,\frac{1}{2}\rangle$
BS_5 = $\begin{bmatrix}\downarrow & & \uparrow\\ & \uparrow & \\ \uparrow & & \downarrow\end{bmatrix}$	$\frac{11}{4}$	$2J_2$				$\frac{1}{\sqrt{10}}\lvert 1,1,2,\frac{5}{2}\rangle + \frac{1}{\sqrt{3}}\lvert 1,1,1,\frac{3}{2}\rangle - \frac{1}{\sqrt{15}}\lvert 1,1,2,\frac{3}{2}\rangle - \frac{1}{\sqrt{6}}\lvert 1,1,1,\frac{1}{2}\rangle + \frac{1}{\sqrt{3}}\lvert 1,1,0,\frac{1}{2}\rangle$

B. Illustration I: {$CuCu_4$} system

Here we have $s_A = s_{B_i} = \frac{1}{2}$. Five distinct states ($BS_i$, $i = 1, 5$) can be obtained by the application of the spin-flip operators (11) onto the high-spin (HS) state ($S = \frac{5}{2}$, it is favored by the ferromagnetic coupling constants, $J_1 > 0$ and $J_2 > 0$) as listed in Table I. However, one of them was not possible to converge, therefore, only HS and BS_1,..., BS_4 are included in the analysis (their energies are in the fifth column of the table, and they are depicted as the first column of Fig. 2). Let us compare three different interpretations of the DFT results. The first possibility is to assume that density functional theory yields physically wrong states without a well defined $\hat{\mathbf{S}}^2$ (the exact composition is presented in the last column of the table, a fitting using this assumption is shown as the second column in the figure). Alternatively, one can accept the arguments of Perdew *et al.* [19] that DFT yields physically correct states, however, the obtained spin density is meaningless and the on-top density is the only relevant observable. In this approach, one still needs to identify the states somehow. This is achieved in columns three and four of the figure. Thus, in our second approach, two doublets and two quartets are selected (indicated in the column 3 of Fig. 2) as to minimize the mean-square error

$$\delta_{\mathrm{RMSE}} = \sqrt{\frac{1}{n}\sum_{i=1}^{n}\left(E_i^{\mathrm{bs}} - E_i^{\mathrm{ex}}\right)^2}, \tag{13}$$

where E_i^{bs} and E_i^{ex} refer to the energies of n states from the broken symmetry approach and the spin-exchange Hamiltonian, respectively. Finally, in the third approach we select the states according to the probability of their participation in each given BS state (indicated in the column 4 of Fig. 2). This is a well-grounded assumption: one can assume that BS states are just initial guesses for DFT, and that in the course of self-consistent calculations the system converges to the physically correct states. The last two fittings produce very similar results, only the interpretation of the second lowest state being different.

As can be seen from Fig. 2, the assumption that DFT yields BS states without a well defined $\hat{\mathbf{S}}^2$ leads to an order of magnitude more precise fitting: $\delta_{\mathrm{RMSE}} = 0.4$ meV vs 6.4 and 7.9 meV, respectively. It has some profound physical implications, and is one of our most important conclusions here. It suggests, that electronic states of DFT theory are very similar to the UHF states (but the two methods yield very different energies), and that spin density is not a completely arbitrary quantity. Thus, our conclusion is that spin projection needs to be done for DFT in the same ways it is done for UHF. So far, this is a statement on the basis of one DFT calculation for a single system. Illas *et al.* [37] made similar claims "it is demonstrated that the last supposition (one accepts the DFT energy of the BS solution and disregards the qualitatively incorrect $\hat{\mathbf{S}}^2$ and spin density), although perhaps numerically acceptable, leads to contradictions with the rigorous first-principles point

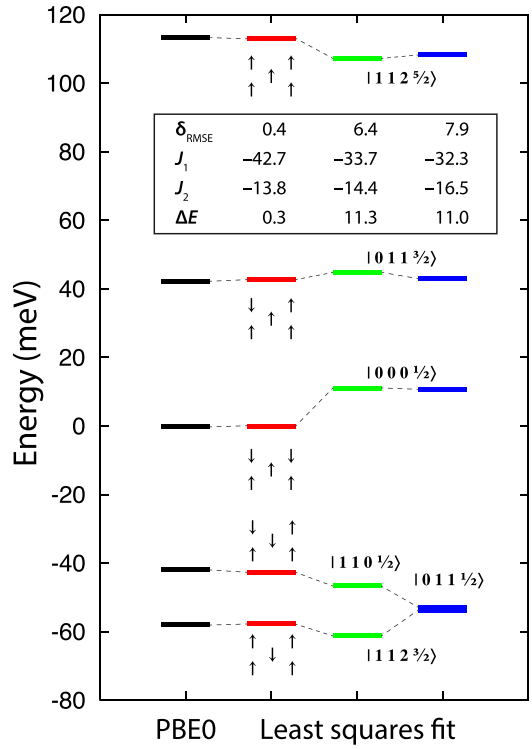

FIG. 2. Comparison of different fitting approaches against "exact" *ab initio* values (black, first column). Second column (red) shows energy levels from the projection approach as described in Table I. This is the most accurate method as can also be concluded from the lowest mean-square error (inset table, all values are in meV). Third and fourth columns show the results of fitting by the eigenstates of the Heisenberg Hamiltonian, best and most probable fits, respectively. Experimental values of the exchange coupling constants are $J_1 = -19.24$ meV and $J_2 = -11.44$ meV [10].

of view." However, their results for spin dimers, although in line with our observations, in principle cannot lead to a conclusive statement. Let us consider another system and functionals.

C. Illustration II: {CuFe$_4$} system

Here, we have $s_A = \frac{1}{2}$ and $s_{B_i} = \frac{5}{2}$. Five states (BS$_i$, $i = 1, 5$) can be obtained by the application of the spin-flip operators on the high-spin state $S = \frac{21}{2}$. It is not feasible to list the composition of all the states; they are too numerous: the Hilbert space decomposes as

$$\begin{aligned}\tfrac{1}{2}\otimes\left[\tfrac{5}{2}\otimes\tfrac{5}{2}\otimes\tfrac{5}{2}\otimes\tfrac{5}{2}\right] = {}& \tfrac{1}{2}^{21}\oplus\tfrac{3}{2}^{36}\oplus\tfrac{5}{2}^{45}\oplus\tfrac{7}{2}^{48}\oplus\tfrac{9}{2}^{45}\\ &\oplus\tfrac{11}{2}^{36}\oplus\tfrac{13}{2}^{25}\oplus\tfrac{15}{2}^{16}\\ &\oplus\tfrac{17}{2}^{9}\oplus\tfrac{19}{2}^{4}\oplus\tfrac{21}{2},\end{aligned}\tag{14}$$

where $S_A \otimes S_B$ and $S_A \oplus S_B$ is a direct product and a direct sum of two spin representations of dimensions $2S_A + 1$ and $2S_B + 1$, respectively. The superscript specifies the number of independent multiplets of each spin. Therefore, in the last column of Table II, only the probabilities of states to have a certain value of total spin, $S = \frac{1}{2}, \ldots, \frac{21}{2}$, are indicated. They were obtained by using the prescription (6).

As an alternative fitting scenario, we also considered eigenstates that have the highest participation in the BS states. In contrast to the BS states, they are physically correct states having a well-defined spin. It turns out, however, that in line with results for CuCu$_4$, the first interpretation is much more precise. The fitting errors are $\delta_{\mathrm{RMSE}} = 1.294$ and 7.220 meV, respectively. Here, we have not searched for a subset of states yielding the best possible fit as was done in the previous example. The reason is that for such large number of states, a good matching could also be found, but it will not be a physically motivated solution. Thus, our second example also indicates that BS DFT calculations should be interpreted in terms of the Noodleman-Dai-Whangbo approach [16,17].

This does not exclude a possibility that with improved density functionals, the suggestion of Perdew *et al.* [19] that DFT yields physically correct states, but meaningless spin density, is valid. Concerning the numerical values of the exchange-coupling constants, we are very much in line with the conclusions of Illas *et al.* [37]: the results of fitting using the above assumption yield values surprisingly close to experimental ones ($J_1 = -6.684$ meV and $J_2 = -0.329$ meV vs $J_1 = -6.10$ meV and $J_2 = -0.47$ meV [10]), however, for a wrong reason. A comparison of the fitting errors suggests that values based on the BS assumptions $J_1 = -7.228$ meV and $J_2 = -0.191$ meV should be used. The remaining discrepancies with experiment are attributed to the insufficiency of the PBE0 functional, which leads to the overestimation of the exchange-coupling constants as has also been observed for the CuCu$_4$ molecule.

D. *g* tensors of broken symmetry states

Now, we add relativistic effects to our Hamiltonian parametrized in terms of the g and D tensors:

$$\hat{\mathcal{H}}_{\mathrm{S}} = \mu_B \mathbf{B}\cdot g\cdot\hat{\mathbf{S}} + \underbrace{\hat{\mathbf{S}}\cdot D\cdot\hat{\mathbf{S}}}_{\hat{\mathcal{H}}_{\mathrm{ZFS}}}.\tag{15}$$

This is the most general form of an interaction of spins with a magnetic field $\mathbf{B}$, *linear* in $\mathbf{B}$ and $\hat{\mathbf{S}}$, and a *bilinear* interaction of spins and can simultaneously be regarded as the definition of corresponding g and D tensors.

Equation (15) characterizes the system as whole. This is also the experimental scenario, and the way how g and D tensors are computed *ab initio* (some details of this procedure are presented in Sec. II E). It is quite obvious that results may depend to some extent on the nature of the system state, for which these properties are computed. The interpretation of high-spin states does not lead to any ambiguities. Perdew's interpretation of the BS states is likewise unambiguous. However, if these states do not have a well-defined total spin, information about the observed g tensor has to be inferred from the partial data. To the best of our knowledge, this dichotomy has not been sufficiently emphasized before. Slep *et al.* [46] used BS solutions for the Fe$^{\mathrm{IV}}$Fe$^{\mathrm{III}}$ complex in order to derive properties of states with well-defined spin. However, they do not provide a solution for more than two magnetic centers. Moreover, different possibilities for the interpretation of BS DFT solutions are not discussed. These are the gaps that will be filled in below.

TABLE II. Excited states of the $CuFe_4$ system from the broken symmetry approach. Numerical data from the PBE0 DFT BS calculations. In the fourth column a constant −8937.0 Hr is subtracted, the values in the fifth column are with respect to the BS_4 state. The least-squares fit yields $J_1 = -7.228$ meV and $J_2 = -0.191$ meV with the root-mean-square error $\delta_{\mathrm{RMSE}} = 1.294$ meV. In the last columns, probabilities p_S of occupying a state with total spin $S = \frac{1}{2}, \ldots, \frac{21}{2}$ are given. We have $\langle \hat{\mathbf{S}}^2 \rangle = \sum_S p_S S(S+1)$.

State	$\langle \hat{\mathbf{S}}^2 \rangle$	$\langle \widehat{\mathcal{H}}_{\mathrm{ex}} \rangle$	E (Hr)	E (meV)	E^{fit} (meV)	p_S
HS = $\begin{bmatrix}\Uparrow & & \Uparrow \\ & \uparrow & \\ \Uparrow & & \Uparrow\end{bmatrix}$	$\frac{483}{4}$	$-10(J_1+5J_2)$	−0.9760438360	85.307	84.664	1
BS_1 = $\begin{bmatrix}\Uparrow & & \Uparrow \\ & \downarrow & \\ \Uparrow & & \Uparrow\end{bmatrix}$	$\frac{403}{4}$	$10(J_1-5J_2)$	−0.9813651089	−59.493	−59.903	$\frac{20}{21}$ $\frac{1}{21}$
BS_2 = $\begin{bmatrix}\Downarrow & & \Uparrow \\ & \uparrow & \\ \Uparrow & & \Uparrow\end{bmatrix}$	$\frac{163}{4}$	$-5J_1$	−0.9777419909	39.098	38.969	$\frac{12}{17}$ $\frac{35}{153}$ $\frac{160}{2907}$ $\frac{3}{323}$ $\frac{20}{20349}$ $\frac{1}{20349}$
BS_3 = $\begin{bmatrix}\Downarrow & & \Uparrow \\ & \downarrow & \\ \Uparrow & & \Uparrow\end{bmatrix}$	$\frac{123}{4}$	$5J_1$	−0.9803812421	−32.720	−33.314	$\frac{5}{8}$ $\frac{9}{34}$ $\frac{35}{408}$ $\frac{20}{969}$ $\frac{9}{2584}$ $\frac{5}{13566}$ $\frac{1}{54264}$
BS_4 = $\begin{bmatrix}\Downarrow & & \Downarrow \\ & \uparrow & \\ \Uparrow & & \Uparrow\end{bmatrix}$	$\frac{43}{4}$	0	−0.9791787989	0.000	2.828	$\frac{1}{6}$ $\frac{10}{39}$ $\frac{45}{182}$ $\frac{16}{91}$ $\frac{5}{52}$ $\frac{9}{221}$ $\frac{35}{2652}$ $\frac{40}{12597}$ $\frac{9}{16796}$ $\frac{5}{88179}$ $\frac{1}{352716}$
BS_5 = $\begin{bmatrix}\Downarrow & & \Uparrow \\ & \uparrow & \\ \Uparrow & & \Downarrow\end{bmatrix}$	$\frac{43}{4}$	$50J_2$	−0.9793872916	−5.673	−6.725	$\frac{1}{6}$ $\frac{10}{39}$ $\frac{45}{182}$ $\frac{16}{91}$ $\frac{5}{52}$ $\frac{9}{221}$ $\frac{35}{2652}$ $\frac{40}{12597}$ $\frac{9}{16796}$ $\frac{5}{88179}$ $\frac{1}{352716}$

As a basis for our derivations, we will be using a general approach for the treatment pairs of spins (let us denote them as $\hat{\mathbf{s}}_a$ and $\hat{\mathbf{s}}_b$) by Bencini and Gatteschi [45] (Chap. 3 is relevant). They consider spin levels in the strong exchange limit that is also relevant for our two systems.[1] Let g_a and g_b be the g tensors pertinent to each magnetic subsystem. Our goal is to derive an *effective* g tensor for the whole system. This is done by demanding that matrix elements of the effective Hamiltonian and the Hamiltonian of the composite system are equal:

$$\langle s'm'|\hat{\mathcal{H}}_{\mathrm{S}}|sm\rangle \doteq \langle s'm'|\hat{\mathcal{H}}_{\mathrm{S}}^{(A)} + \hat{\mathcal{H}}_{\mathrm{S}}^{(B)}|sm\rangle. \tag{16}$$

Matrix elements

$$\begin{aligned}\langle s'm'|\hat{\mathcal{H}}_{\mathrm{S}}|sm\rangle &= \langle s'm'|\mu_B(\mathbf{B}\cdot g_a\cdot\hat{\mathbf{s}}_a + \mathbf{B}\cdot g_b\cdot\hat{\mathbf{s}}_b)|sm\rangle \\ &= \tfrac{1}{2}\mu_B\langle s'm'|\mathbf{B}\cdot g_+\cdot\hat{\mathbf{s}}_0 + \mathbf{B}\cdot g_-\cdot\hat{\mathbf{v}}|sm\rangle \end{aligned}\tag{17}$$

are relevant. Here, $g_\pm = g_a \pm g_b$, $\hat{\mathbf{s}}_0 = \hat{\mathbf{s}}_a + \hat{\mathbf{s}}_b$, and $\hat{\mathbf{v}} = \hat{\mathbf{s}}_a - \hat{\mathbf{s}}_b$. $|sm\rangle$ can be expressed in terms of $|s_A m_A\rangle$ and $|s_B m_B\rangle$ by the inverse of Eq. (2) (spin addition). We can write

$$g = \tfrac{1}{2}(c_+ g_+ + c_- g_-). \tag{18}$$

The part containing g_+ has already the right form as in Eq. (15), therefore, $c_+ = 1$. For c_- we can use the Wigner-Eckart theorem

$$c_- = \frac{\langle sm'\tau'|\hat{\mathbf{v}}|sm\tau'\rangle}{\langle sm'\tau'|\hat{\mathbf{s}}_0|sm\tau\rangle} = \frac{\langle s\tau'\|\hat{\mathbf{v}}\|s\tau\rangle}{\langle s\tau'\|\hat{\mathbf{s}}_0\|s\tau\rangle}, \tag{19}$$

where $\langle s\tau'\|T_k\|s\tau\rangle$ is a general notation for the reduced matrix elements of the *irreducible tensor operators* (for the present application the rank k will never exceed 1). τ indicates the intermediate quantum numbers [$\tau = \{s_a, s_A, s_b, s_B\}$ in Eq. (6)].

Matrix elements of $\hat{\mathbf{v}}$ are evaluated applying the equation for tensor products [Eq. (7.1.5) of Edmonds [49]] twice, for $\hat{\mathbf{s}}_a \otimes \hat{I}$ and $\hat{I} \otimes \hat{\mathbf{s}}_b$ (with ranks equal 1 in both cases, $\hat{I}$ is the identity operator), respectively,

$$c_- = \frac{s_a(s_a+1) - s_b(s_b+1)}{s(s+1)}. \tag{20}$$

Having essentially replicated the derivation of Bencini and Gatteschi, let us inspect what modifications would be needed in the case of several (more than 2) magnetic centers (spins).

In $\langle sm'\tau'|\hat{\mathbf{v}}|sm\tau'\rangle$, $\hat{\mathbf{s}}_a$ and $\hat{\mathbf{s}}_b$ are just spin operators acting only on the respective subsystems. In view of

$$\langle s\tau\|\hat{\mathbf{s}}_0\|s'\tau'\rangle = \delta_{\tau\tau'}\delta_{ss'}\sqrt{s(s+1)(2s+1)}, \tag{21}$$

there is no dependence on the intermediate quantum states for *reduced* matrix elements at marked variance with overlap integrals, which lead to the appearance of *recoupling coefficients* [cf. Eq. (5)]. Therefore, the main equations (18) and (20) can be used in a more general context, for instance, by building up the AB_4 spin system as indicated by Eq. (9). Thus, the Wigner-Eckart theorem leads to a great simplification for multispin systems, and allows to write for the AB_4 spin model

[1]The magnitude of Zeeman splitting is determined by the strength of the magnetic field. Measurements for the two systems have been performed at Heidelberg University and reported in the thesis of Park [38] for fields as high as 16 T. The ESR splitting was typically in the range of several hundred GHz, i.e., $1 \div 2$ meV, which is smaller than level spacing in Tables I and II.

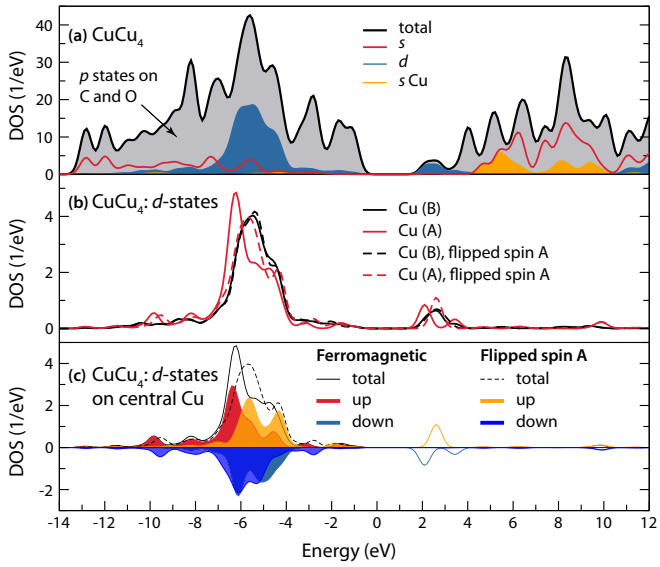

FIG. 3. (a) Partial density of states of the $CuCu_4$ system in the valence region, where the main contribution is mostly due to the p states localized on the C and O atoms. (b) Magnetically important d states are split into a pronounced occupied peak in the region -7 to -4 eV and one partially occupied peak in the region 2 to 4 eV. With the help of the Löwdin population analysis, the evolution of the electron density upon the spin flip on the central Cu^{II} ion (BS_1) can be visualized (c).

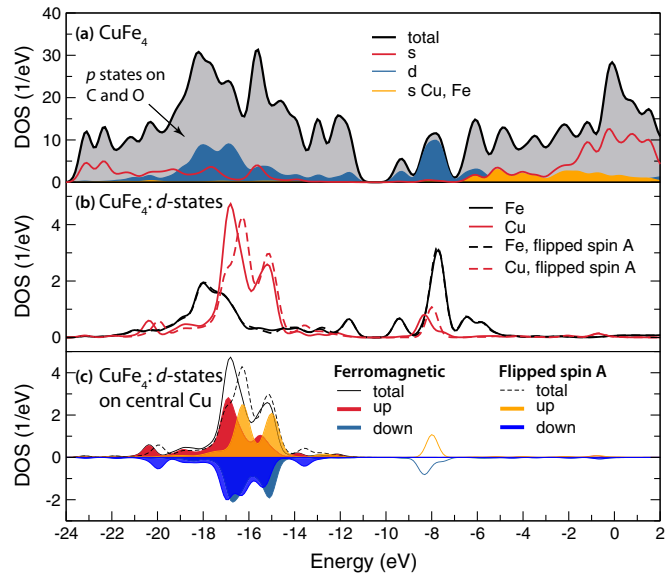

FIG. 4. (a) Partial density of states of the $CuFe_4$ system in the valence region, where the main contribution is mostly due to the p states localized on C and O atoms. (b) Magnetically important d states are split into a pronounced occupied peak in the region -20 to -14 eV and one partially occupied peak in the region -9 to -6 eV. With the help of the Löwdin population analysis, the evolution of the electron density upon the spin flip on the central Cu^{II} ion (BS_1) can be visualized (c).

in the $|S_{13}, S_{24}, S_B, S, M_S\rangle$ eigenstate:

$$g = \frac{1}{2}(g_a + g_b) + \frac{s_a(s_a+1) - s_B(s_B+1)}{2S(S+1)}(g_a - g_b). \quad (22)$$

For BS states the orthogonality and the expansion coefficients are needed.

E. *Ab initio* calculations

In the preceding section we presented numerical results for the PBE0 functional of Ernzerhof and Scuseria [50] and by Adamo and Barone [51], which is hybrid of PBE exchange and correlation GGA functional with 25% of Fock exchange. The corresponding density of states is shown for the two systems in Figs. 3 and 4. Comparing these two figures, it can be observed that the d band is narrower in $CuCu_4$ than in $CuFe_4$ because the energy difference between the Cu and the Fe d states in the heterometallic complex is larger than between the central and the peripheral Cu ions in $CuCu_4$. Results on Figs. 3(a) and 4(a) correspond to the ground states for the fully aligned spins with $S = \frac{5}{2}$ and $\frac{21}{2}$, respectively. Flipping of the central spin (we are talking about the BS_1 states here) has small but visible impact on the electronic structure in both cases [panels (b) and (c) of the respective figures]. The majority-spin band shifts to higher energies, the unoccupied peak changes its character from spin up to spin down.

Ab initio calculations in this work were performed using the Kohn-Sham methods as implemented in the ORCA quantum chemistry program [52]. Relativistic calculations are the major part of this package. Only briefly we mention that theory of g-tensor calculations (and here we mean the interplay of many-particle and relativistic aspects) was developed in numerous works. For a comprehensive review of the literature prior to 2009 we refer to the paper of Gauss *et al.* [53]. From this work we can learn in particular that a general formulation of theory is due to McWeeny [54]. Accordingly, aside from the bare free-electron value of the tensor, there are three contributions: paramagnetic spin-orbit (pso), diamagnetic spin orbit (dso), and relativistic mass correction (rmc). The latter two are simple expectation values that can be determined from the known wave functions. The paramagnetic contribution, which is also the largest one, is a second-order effect. It results from the modification of the total energy due to the combination of (i) the magnetic field interacting with the electron orbital moment and (ii) the spin-orbit interaction:

$$g_{\rm pso} = \frac{1}{\mu_B}\left(\frac{\partial^2 E}{\partial \mathbf{B}\partial \mathbf{S}}\right)_{\mathbf{B},\mathbf{S}=0}, \quad (23)$$

where the two constituents are

$$\hat{\mathcal{H}}_{\rm b} = \mu_B \mathbf{B}\cdot\mathbf{L}, \quad (24)$$

$$\hat{\mathcal{H}}_{\rm SOC} = \frac{\alpha^2}{2}\sum_i\sum_A Z_A \frac{(\mathbf{r}_i - \mathbf{R}_A)\times\mathbf{p}_i}{|\mathbf{r}_i - \mathbf{R}_A|^3}\cdot\hat{\mathbf{s}}_i - \frac{\alpha^2}{2}\sum_i\sum_{j\neq i}\frac{(\mathbf{r}_i - \mathbf{r}_j)\times\mathbf{p}_i}{|\mathbf{r}_i - \mathbf{r}_j|^3}\cdot(\hat{\mathbf{s}}_i + 2\hat{\mathbf{s}}_j). \quad (25)$$

Here, $\mathbf{r}$, $\mathbf{p}$, and $\hat{\mathbf{s}}$ are position, momentum, and spin operators of an electron, $\alpha = 1/c$ is the fine-structure constant. $\mathbf{R}_A$ denotes positions of nuclei with corresponding charge Z_A.

A standard way of computing the derivatives of the total-energy expectation value is by using the coupled perturbed

Kohn-Sham theory. We refer here to the original work of Neese [55] for all the details of this approach.

There are several complications that arise in practical calculations. One of them is the treatment of spin-orbit coupling [47]. Already from Eq. (25), it is clear that there are one-electron (first term) and two-electron (second term) contributions. If, furthermore, density functional theory is used, different forms of exchange and correlations need to be taken into account. This is nicely summarized in Fig. 1 of Ref. [56]. Another important aspect is the treatment of relativistic effects with magnetic field at second-order Douglas-Kroll-Hess (DKH) level. The importance of including the magnetic field from the beginning into the Foldy-Wouthuysen transformation was established in Ref. [57].

III. RESULTS

In this section we continue our investigation of the $CuCu_4$ and $CuFe_4$ metallacrowns by systematically employing different exchange-correlation functionals. In Sec. III A, we visualize the electronic structure of the heterometallic system in energy and in space domains providing more insight into the states in Table II. These data are essential for the interpretation of the scanning tunneling spectroscopy and the time- and spin-resolved photoemission experiments which are anticipated in future, and it is used in analyzing the dependence of the g tensors on the spin localization. In Sec. III B we make a connection with experimental measurements performed at Heidelberg university [38]. Their main findings are $g^{\mathrm{iso}} = 2.05$, and $g_\perp = 2.03$, $g_\parallel = 2.23$ for the $CuCu_4$ compound.

A. More on the electronic structure

Before presenting our results for the g tensor, we would like to clarify the electronic structure of various broken symmetry solutions of the Kohn-Sham equation. In Tables I and II the theoretical compositions of these states are presented, and in Figs. 3 and 4 the impact of the spin flip on the central TM ions is demonstrated. These theoretical predictions can be compared with two general scenarios how the electronic and spin systems respond during the ferromagnetic-paramagnetic phase transition as discussed by Eich *et al.* [58]. It was suggested that for itinerant electrons, the magnetic moments are quenched via single-particle transitions that induce a collapse of the exchange splitting and therefore a shift of the spin-polarized bands. This is clearly not the case here although tiny shifts are indeed visible. However, the second scenario, pertinent to localized systems, is more appropriate here. There is, however, one very important difference between theoretical calculations and experimental observations using time-resolved photoelectron spectroscopy. In the latter case, because experiment only probes the macroscopic average of spin fluctuations, one observes the so-called band mirroring effect, i. e., spin up and down densities of states are nearly identical. The theory, of course, observes a frozen picture, where spin up and spin down states are occupied differently.

It is of interest to perform this analysis in greater details. The Löwdin reduced orbital population analysis [59] of the PBE0 results is represented in the form of the partial density of states (DOS) for $CuFe_4$ (Fig. 5). The shifts in the position of Cu d states of about 1 eV and the redistribution of the electronic density on Fe d states can be seen for both occupied and unoccupied states (the position of the Fermi level is different for both clusters because of the different charge states adopted in both calculations). At the same time, the spin flipping on the Cu^{II} ion results only in a small modification of the electronic density on Fe^{III} (and vice versa). This fact can be attributed to an almost vanishing overlap of the d states on different transition metal ions and is visualized for different broken symmetry states in Fig. 1.

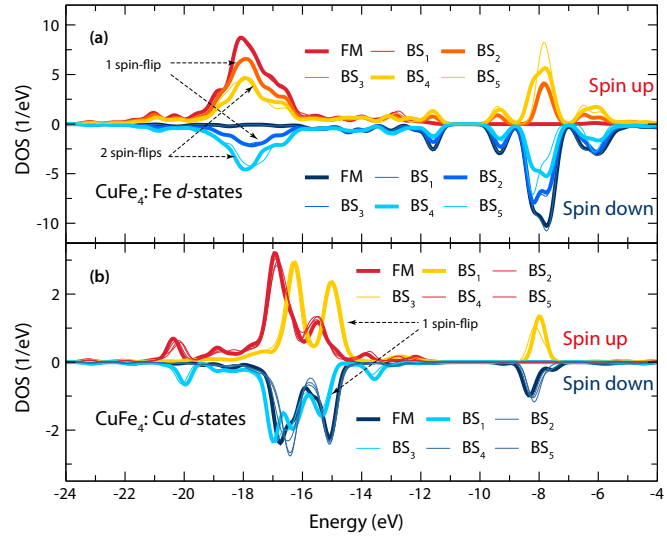

FIG. 5. Partial density of d states of the $CuFe_4$ system in the valence region due to Fe^{III} (a) and Cu^{II} (b) ions. Five broken symmetry states (Table II) are compared with the ferromagnetic state ($S = \frac{21}{2}$), which is the reference state. The states are grouped according to the number of Fe (top) and Cu (bottom) ions with flipped spins and depicted with the same color. Flipping the spin on the Cu^{II} ion results in only small density modification on the Fe^{III} (and vice versa), and therefore is not distinguished by the line style.

Another interesting fact that can be inferred from the population analysis in Fig. 5(b) is the quite strong redistribution of the electron density upon a spin flip on the central Cu^{II} ion. Aside from the shift of about 1 eV, some portion of the spectral weight is transferred to higher energies enhancing the magnitude of the second peak. While this can be an indication of the $d_{z^2} \rightarrow d_{x^2-y^2}$ transition on the central Cu^{II} ion, we cannot clearly separate contributions of various symmetry-adapted d orbitals in the density of states. In principle, such an effect can be observed spectroscopically (see introduction to Ref. [61] for a list of spectroscopic techniques applied to magnetic molecules), however, due to the fact that the exchange constants J_1 and J_2 are very small, both electronic states are thermally populated and cannot be discriminated. Recently, observation and electric current control of a local spin in a single-molecule magnet $TbPc_2$ absorbed on an Au(111) surface have been demonstrated [62]. However, in this experiment, the Kondo resonance originates from an unpaired spin in a π orbital of ligands rather than from the local magnetic moment of metal ion. Therefore, more detailed spectroscopic investigations are expected in the future. The

TABLE III. Exchange-coupling constants for the $CuCu_4$ homometallic metallacrown obtained using different methods. The experimental results are reported in Happ *et al.* [60], the results of wave-function methods, the complete active space (CAS) and the second-order perturbation theory (NEVPT2), are reported in Pavlyukh *et al.* [9].

Method	J_1 (meV)	J_2 (meV)
CAS(5,5)	−2.70	−0.90
NEVPT2	−6.36	−2.08
PBE0	−42.7	−13.8
Experiment	−19.24	−11.4

feasibility of the spin- and time-resolved scanning tunneling spectroscopy of magnetic adatoms on surfaces was discussed by Schüler *et al.* [63,64], and a recent experimental review is by Ternes [65].

Thanks to comprehensive experiments [60], we now have a detailed knowledge of the exchange-coupling constants in the studied metallacrowns. In the preceding section we focused on the physical nature of the broken symmetry states and on the consistency of their energy levels. Further results will be presented below comparing different exchange-correlation functionals. However, it is also instructive to put our best DFT results (obtained with PBE0 functional) in relation to the wave-function (WF) methods (Table III). WF methods have an advantage that multiconfigurational character of magnetic states is properly taken into account, alleviating the problem of interpretation of the spin density. However, being more rigid on this point also means less flexibility in the description of electronic correlations, which need to be added on top. Thus we find, in line with other works on molecular magnets of various compositions and number of magnetic centers [36,37], that wave-function methods generally underestimate exchange-coupling constants, whereas density functional methods overestimate them. The ratio between the two exchange-coupling constants J_1/J_2 is systematically overestimated by all considered theories (Table III). We tentatively ascribe this to a higher-order mechanism mediated by the two ligand atoms in the oxamate bridge ON, which is responsible for the formation of antiferromagnetic J_2. In contrast, J_1 is a classical case of the Anderson-Goodenough-Kanamori superexchange with a single hopping.

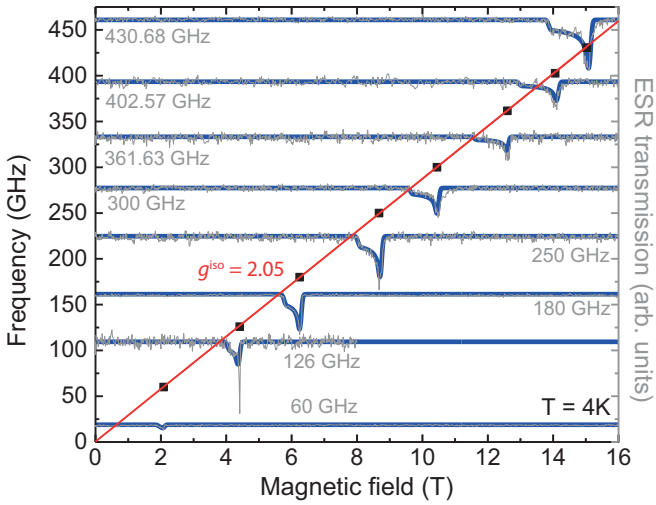

FIG. 6. Determination of the isotropic part and three principal values ($g_1 = 2.03 \pm 0.01$, $g_2 = 2.04 \pm 0.01$, $g_3 = 2.23 \pm 0.01$) of the g tensor by the fitting of the high-field high-frequency electron spin resonance (ESR) measurements for the polycrystalline $CuCu_4$ system. Experimental data (gray lines), model fit (thick blue lines). g^{iso} can be determined from the maxima positions (red line). Extrapolation of the fitting line to zero magnetic field shows no remanent splitting. This indicates vanishing zero-field splitting tensor. The temperature dependence is reflected only in the broadening of the resonances. Above $T = 70$ K, the ESR spectrum disappears. Adapted from Ref. [39].

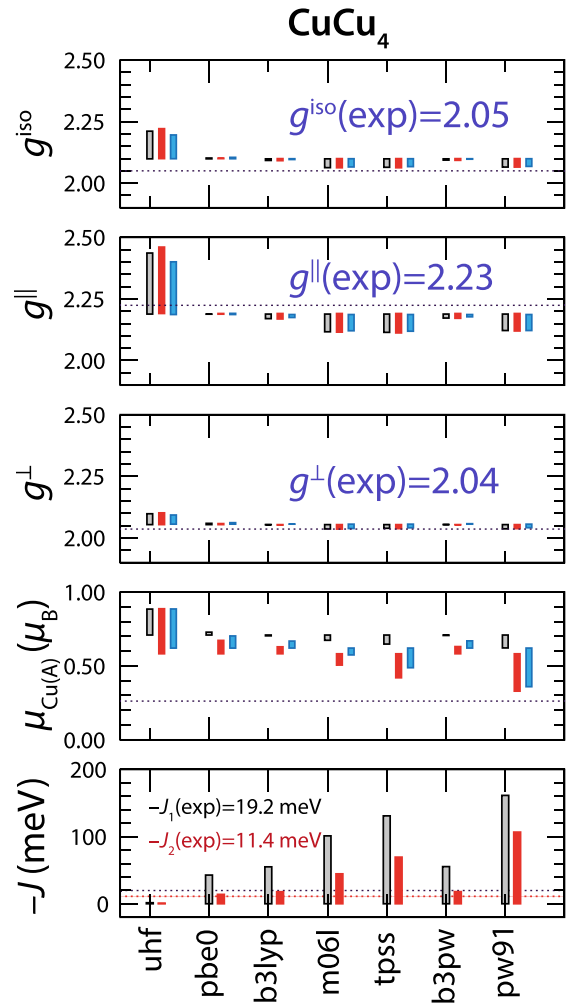

FIG. 7. Computed values of the g tensor, localized spin moments on the central TM ion ($\mu_{Cu(A)}$) and spin-exchange-coupling constants J_1 and J_2 for the $CuCu_4$ system. Components of the g tensor (isotropic g^{iso}, out of the molecule plane $g^{\parallel}$, and in-plane $g^{\perp}$) as well as the Löwdin spin moments of the central Cu^{II} are plotted for three states (HS, BS_1, BS_4) and color coded as gray, red, and blue bars. Averages over all the functionals serve as the reference values. Thus, the size of the bars indicates the deviation from the reference value. Experimental values are indicated as dotted lines as well. In the lowest panel, the exchange-coupling constants J_1 (gray) and J_2 (red) are indicated for each DFT functional.

B. *g* tensor of $CuCu_4$

Experimental results are summarized in Fig. 6. We refer to Park [38] for all the details and to Fedin *et al.* [66] for a review on the electron paramagnetic resonance of copper-based molecular magnets. Raw computational data are presented and various relativistic options are discussed in the Supplemental Material [47]. We find that a graphical representation of these data such as on Fig. 7 yields the most lucid picture. While different exchange-correlation functionals generally provide consistent results, there are some marked differences. First, we notice that unrestricted Hartree-Fock is never a good choice: it substantially overestimates the *g* tensors, underestimates the exchange-coupling constants as was already pointed out in Table III, and yields spins fully localized on TM ions (Löwdin spins differ only slightly from integer values expected from a simple coordination chemistry picture). The latter is in qualitative (considering limitations of the Löwdin population analysis) disagreement with the measured (by the x-ray magnetic circular dichroism) magnetic moments ($\mu = 0.27 \pm 0.02$ for the central Cu^{II} ion) [60].

Spin values vary substantially for different functionals, and some correlations between the spin localization and the *g* tensor, J_1 and J_2, can be observed: more localized spins imply smaller values of the exchange constants and larger *g*-tensor values, and vice versa. The PW91 functional is rather inaccurate in this respect, the spins are weakly localized leading to smaller than experimental values of *g* and to very large values of the exchange coupling. At the same time, all functionals yield very similar values of *g* for different excited states, which probably explains why fitting of the experimental ESR measurements was so consistent.

IV. CONCLUSIONS

In this work we investigated two metallacrown molecules $CuCu_4$ and $CuFe_4$ as paradigmatic systems to discuss (i) the extraction of exchange-coupling constants using the broken symmetry approach of the density functional theory and (ii) the calculation of relativistic properties such as the *g* tensor. Both systems have frustrated antiferromagnetic ground states, which result from the interplay of the antiferromagnetic coupling between the central and the peripheral TM ions and much weaker antiferromagnetic couplings between the peripheral ions and are driven by the superexchange mechanism [5]. Corresponding electronic states can be mimicked by performing constrained calculations as to have a correct open-shell low-spin configuration. However, the question about the total spin moment of such states still needs to be answered. By performing calculations for the redundant number of excited states, we established that they are not eigenstates of the total spin operator, which is against the expectation for the density functional theory to yield physically sensible states [19]. However, such scenario can be anticipated on the basis of numerous calculations for two-center magnetic systems performed in other works [18,37], and can be traced back to the fact that theory in Ref. [19] admits no noninteracting Kohn-Sham system (is not noninteracting v representable) and, ultimately, to the nonuniqueness problem of the spin DFT [67].

Then, we developed a theory for the calculation of *g* tensors starting from the broken symmetry approach. It generalizes early results of Bencini and Gatteschi for the two-center systems. Finally, systematic investigations using different exchange-correlation functionals were performed. We found correlations between the value of the *g* tensor and the effective spins localized on TM ions. Good agreement with experiment was established for the $CuCu_4$ homometallic metallacrown.

ACKNOWLEDGMENT

This work is financially supported by the German Research Foundation (DFG) Collaborative Research Centre SFB/TRR 173 "Spin+X.".

[1] W. Hübner, Y. Pavlyukh, G. Lefkidis, and J. Berakdar, Phys. Rev. B **96**, 184432 (2017).
[2] S. J. Blundell, Contemp. Phys. **48**, 275 (2007).
[3] A. Furrer and O. Waldmann, Rev. Mod. Phys. **85**, 367 (2013).
[4] P. Happ, C. Plenk, and E. Rentschler, Coord. Chem. Rev. **289-290**, 238 (2015).
[5] P. W. Anderson, Phys. Rev. **79**, 350 (1950).
[6] J. B. Goodenough, *Magnetism and the Chemical Bond*, Interscience Monographs on Chemistry (Interscience, New York, 1963).
[7] A. Palii, B. Tsukerblat, S. Klokishner, K. R. Dunbar, J. M. Clemente-Juan, and E. Coronado, Chem. Soc. Rev. **40**, 3130 (2011).
[8] J. P. Malrieu, R. Caballol, C. J. Calzado, C. de Graaf, and N. Guihéry, Chem. Rev. **114**, 429 (2014).
[9] Y. Pavlyukh, E. Rentschler, H. J. Elmers, W. Hübner, and G. Lefkidis, Phys. Rev. B **97**, 214408 (2018).
[10] P. Happ and E. Rentschler, Dalton Trans. **43**, 15308 (2014).
[11] D. Muñoz, F. Illas, and I. de P. R. Moreira, Phys. Rev. Lett. **84**, 1579 (2000).
[12] D. I. Lyakh, M. Musiał, V. F. Lotrich, and R. J. Bartlett, Chem. Rev. **112**, 182 (2011).
[13] P.-O. Löwdin, Phys. Rev. **97**, 1509 (1955).
[14] P. Piecuch, R. Toboła, and J. Paldus, Phys. Rev. A **54**, 1210 (1996).
[15] D. J. Thouless, Nucl. Phys. **21**, 225 (1960).
[16] L. Noodleman and E. R. Davidson, Chem. Phys. **109**, 131 (1986).
[17] M.-H. Whangbo, H.-J. Koo, and D. Dai, J. Solid State Chem. **176**, 417 (2003).
[18] E. Ruiz, J. Cano, S. Alvarez, and P. Alemany, J. Comput. Chem. **20**, 1391 (1999).
[19] J. P. Perdew, A. Savin, and K. Burke, Phys. Rev. A **51**, 4531 (1995).
[20] J. Baker, A. Scheiner, and J. Andzelm, Chem. Phys. Lett. **216**, 380 (1993).
[21] E. Ruiz, A. Rodríguez-Fortea, J. Cano, S. Alvarez, and P. Alemany, J. Comput. Chem. **24**, 982 (2003).
[22] E. Ruiz, A. Rodríguez-Fortea, J. Cano, and S. Alvarez, J. Phys. Chem. Solids **65**, 799 (2004).

[23] J. Kortus, C. S. Hellberg, and M. R. Pederson, Phys. Rev. Lett. **86**, 3400 (2001).
[24] V. Bellini and M. Affronte, J. Phys. Chem. B **114**, 14797 (2010).
[25] V. Bellini, G. Lorusso, A. Candini, W. Wernsdorfer, T. B. Faust, G. A. Timco, R. E. P. Winpenny, and M. Affronte, Phys. Rev. Lett. **106**, 227205 (2011).
[26] A. Chiesa, S. Carretta, P. Santini, G. Amoretti, and E. Pavarini, Phys. Rev. Lett. **110**, 157204 (2013).
[27] A. Chiesa, S. Carretta, P. Santini, G. Amoretti, and E. Pavarini, Phys. Rev. B **94**, 224422 (2016).
[28] E. Ruiz, S. Alvarez, J. Cano, and V. Polo, J. Chem. Phys. **123**, 164110 (2005).
[29] C. Adamo, V. Barone, A. Bencini, R. Broer, M. Filatov, N. M. Harrison, F. Illas, J. P. Malrieu, and I. de P. R. Moreira, J. Chem. Phys. **124**, 107101 (2006).
[30] M. Levy, Phys. Rev. A **26**, 1200 (1982).
[31] M. Filatov and S. Shaik, Chem. Phys. Lett. **288**, 689 (1998).
[32] M. Filatov and S. Shaik, Chem. Phys. Lett. **304**, 429 (1999).
[33] B. Miehlich, H. Stoll, and A. Savin, Mol. Phys. **91**, 527 (1997).
[34] G. Li Manni, R. K. Carlson, S. Luo, D. Ma, J. Olsen, D. G. Truhlar, and L. Gagliardi, J. Chem. Theory Comput. **10**, 3669 (2014).
[35] A. J. Garza, I. W. Bulik, T. M. Henderson, and G. E. Scuseria, Phys. Chem. Chem. Phys. **17**, 22412 (2015).
[36] F. Illas, I. d. P. R. Moreira, J. M. Bofill, and M. Filatov, Theor. Chem. Acc. **116**, 587 (2006).
[37] F. Illas, I. de P. R. Moreira, J. M. Bofill, and M. Filatov, Phys. Rev. B **70**, 132414 (2004).
[38] J. Park, High-field electron spin resonance study on correlated transition metal compounds and metal-organic compounds, Ph.D. thesis, Ruprecht-Karls-Universität Heidelberg, Heidelberg, 2015.
[39] C. Koo, J. Park, J. Butscher, E. Rentschler, and R. Klingeler, J. Magn. Magn. Mater. **477**, 340 (2019).
[40] S. Sharma, K. Sivalingam, F. Neese, and G. K.-L. Chan, Nat. Chem. **6**, 927 (2014).
[41] T. Gupta and G. Rajaraman, Chem. Commun. **52**, 8972 (2016).
[42] A. Chiesa, T. Guidi, S. Carretta, S. Ansbro, G. A. Timco, I. Vitorica-Yrezabal, E. Garlatti, G. Amoretti, R. E. P. Winpenny, and P. Santini, Phys. Rev. Lett. **119**, 217202 (2017).
[43] G. Mezei, C. M. Zaleski, and V. L. Pecoraro, Chem. Rev. **107**, 4933 (2007).
[44] A. Bencini and D. Gatteschi, Mol. Phys. **47**, 161 (1982).
[45] A. Bencini and D. Gatteschi, *Electron Paramagnetic Resonance of Exchange Coupled Systems* (Springer, Berlin, 1990).
[46] L. D. Slep, A. Mijovilovich, W. Meyer-Klaucke, T. Weyhermüller, E. Bill, E. Bothe, F. Neese, and K. Wieghardt, J. Am. Chem. Soc. **125**, 15554 (2003).
[47] See Supplemental Material at http://link.aps.org/supplemental/10.1103/PhysRevB.99.144418 for an overview of the used exchange-correlation functionals and of the relativistic options, which includes Refs. [50,51,56,68–74].
[48] D. Dai and M.-H. Whangbo, J. Chem. Phys. **118**, 29 (2003).
[49] A. R. Edmonds, *Angular Momentum in Quantum Mechanics* (Princeton University Press, Princeton, NJ, 1996).
[50] M. Ernzerhof and G. E. Scuseria, J. Chem. Phys. **110**, 5029 (1999).
[51] C. Adamo and V. Barone, J. Chem. Phys. **110**, 6158 (1999).
[52] F. Neese, Wiley Interdiscip. Rev.: Comput. Mol. Sci. **2**, 73 (2012).
[53] J. Gauss, M. Kállay, and F. Neese, J. Phys. Chem. A **113**, 11541 (2009).
[54] R. McWeeny, J. Chem. Phys. **42**, 1717 (1965).
[55] F. Neese, J. Chem. Phys. **115**, 11080 (2001).
[56] F. Neese, J. Chem. Phys. **122**, 034107 (2005).
[57] B. Sandhoefer and F. Neese, J. Chem. Phys. **137**, 094102 (2012).
[58] S. Eich, M. Plötzing, M. Rollinger, S. Emmerich, R. Adam, C. Chen, H. C. Kapteyn, M. M. Murnane, L. Plucinski, D. Steil, B. Stadtmüller, M. Cinchetti, M. Aeschlimann, C. M. Schneider, and S. Mathias, Sci. Adv. **3**, e1602094 (2017).
[59] A. Szabo, *Modern Quantum Chemistry: Introduction to Advanced Electronic Structure Theory* (Dover, Mineola, NY, 1996).
[60] P. Happ, A. Sapozhnik, J. Klanke, P. Czaja, A. Chernenkaya, K. Medjanik, S. Schuppler, P. Nagel, M. Merz, E. Rentschler, and H. J. Elmers, Phys. Rev. B **93**, 174404 (2016).
[61] A. Mugarza, R. Robles, C. Krull, R. Korytár, N. Lorente, and P. Gambardella, Phys. Rev. B **85**, 155437 (2012).
[62] T. Komeda, H. Isshiki, J. Liu, Y.-F. Zhang, N. Lorente, K. Katoh, B. K. Breedlove, and M. Yamashita, Nat. Commun. **2**, 217 (2011).
[63] M. Schüler, Y. Pavlyukh, and J. Berakdar, New J. Phys. **14**, 043027 (2012).
[64] M. Schüler, Y. Pavlyukh, and J. Berakdar, J. Phys. Chem. Lett. **4**, 1131 (2013).
[65] M. Ternes, Prog. Surf. Sci. **92**, 83 (2017).
[66] M. V. Fedin, S. L. Veber, E. G. Bagryanskaya, and V. I. Ovcharenko, Coord. Chem. Rev. **289-290**, 341 (2015).
[67] U. v. Barth and L. Hedin, J. Phys. C: Solid State Phys. **5**, 1629 (1972).
[68] A. D. Becke, J. Chem. Phys. **98**, 5648 (1993).
[69] C. Lee, W. Yang, and R. G. Parr, Phys. Rev. B **37**, 785 (1988).
[70] J. P. Perdew, J. A. Chevary, S. H. Vosko, K. A. Jackson, M. R. Pederson, D. J. Singh, and C. Fiolhais, Phys. Rev. B **46**, 6671 (1992).
[71] J. Tao, J. P. Perdew, V. N. Staroverov, and G. E. Scuseria, Phys. Rev. Lett. **91**, 146401 (2003).
[72] Y. Zhao and D. G. Truhlar, J. Chem. Phys. **125**, 194101 (2006).
[73] F. Weigend and R. Ahlrichs, Phys. Chem. Chem. Phys. **7**, 3297 (2005).
[74] F. Weigend, Phys. Chem. Chem. Phys. **8**, 1057 (2006).